Advancing Enhanced Weathering Modeling in Soils: Systematic Comparison and Validation with Experimental Data

Matteo B. Bertagni[1,2], Salvatore Calabrese[3], Giuseppe Cipolla[4], Leonardo V. Noto[4], and Amilcare Porporato[1,2]

[1]The High Meadows Environmental Institute, Princeton University, Princeton, NJ, USA
[2]Department of Civil and Environmental Engineering, Princeton University, Princeton, NJ, USA
[3]Department of Biological and Agricultural Engineering, Texas A&M University, College Station, TX, USA
[4]Dipartimento di Ingegneria, Università degli Studi di Palermo, Palermo, Italia

Key Points:

- We present a dynamic, depth-averaged model for enhanced weathering dynamics in the upper soil layers.
- The model is validated with four experimental datasets of different complexity.
- The model-experiment comparison demonstrates slower-than-expected dissolution rates.

Corresponding author: Matteo B. Bertagni, `matteobb@princeton.edu`

Abstract

Enhanced weathering (EW) is a promising strategy to remove atmospheric CO_2 by amending agricultural and forestry soils with ground silicate materials. However, the current model-based assessments of EW potential face uncertainties stemming from the intricate interplay among soil physical, chemical, and biotic processes, compounded by the absence of a detailed model-data comparison, mostly due to the limited availability of comprehensive data. Here, we address this critical gap by advancing and validating an ecohydrological and biogeochemical model for EW dynamics in soils. We conduct a hierarchical validation in which model results are critically compared to four experimental datasets of increasing complexity, from simple closed incubation systems to open mesocosm experiments. The comparison demonstrates the model ability to capture the dynamics of primary variables, including rock alkalinity release and CO_2 sequestration. The comparison also reveals that weathering rates are consistently lower than traditionally assumed by up to two orders of magnitude. We finally discuss avenues for further theoretical and experimental explorations.

Plain Language Summary

Enhanced weathering (EW) is a promising strategy to mitigate climate change while increasing agricultural productivity and mitigating ocean acidification. The strategy involves enriching cropland and forest soils with finely ground silicate rocks, which sequester atmospheric CO_2 upon dissolution. However, current EW assessments relying on models face uncertainty, primarily stemming from challenges in accurately representing the intricate hydrological and biogeochemical processes driving mineral dissolution in the soil. The absence of a robust model-data comparison exacerbates these uncertainties. This study addresses these issues by presenting a model for EW dynamics in the upper soil layer, successfully replicating diverse experimental datasets. Our model reveals a slower mineral dissolution rate than conventionally assumed, offering crucial insights for a comprehensive understanding of EW as a negative emission strategy.

1 Introduction

In addition to emissions reduction from every sector, significant carbon dioxide removal (CDR) through negative emission technologies (NETs) is needed to limit global warming (Calvin et al., 2023). Among various proposed NETs, enhanced weathering (EW) is emerging as one with considerable CO_2 removal potential and low technological requirements (Kohler et al., 2010; Renforth, 2012; Berge et al., 2012; Hartmann et al., 2013; Taylor et al., 2016; Beerling et al., 2020; Calabrese et al., 2022). EW relies on amending agricultural and forestry soil with crushed silicate materials (e.g., basalt, dunite, wollastonite) to promote biomass growth and sequester CO_2 in aqueous or mineral forms (Hartmann et al., 2013; Taylor et al., 2021). Upon dissolution, the hydrologic cycle transports part of the EW products to surface freshwaters and the ocean, mitigating ocean acidification and stably sequestering atmospheric CO_2 for geological timescales (Renforth & Henderson, 2017; Bertagni & Porporato, 2022). As a further co-benefit, EW is expected to improve nitrogen use efficiency (NUE) in agricultural fields, reducing reactive nitrogen emissions and the demand for fossil-fuel-based fertilizers (Blanc-Betes et al., 2021; Val Martin et al., 2023). Deployed over suitable lands at the global scale, it is estimated that EW potential may reach the order of gigatonnes of CO_2 removal per year (Taylor et al., 2016; Strefler et al., 2018; Beerling et al., 2020; Baek et al., 2023).

Despite these promising estimates, EW assessments face significant uncertainties rooted in the complex interplay between hydrological and biogeochemical processes across scales (Calabrese et al., 2022). Weathering rates exhibit considerable variability, spanning orders of magnitudes due to temporal and spatial heterogeneity in hydroclimatic drivers and soil processes (Amann et al., 2020; Calabrese & Porporato, 2020; Deng et

al., 2022). This variability complicates efforts to reconcile theoretical expectations with laboratory observations, even for the same rock type (Renforth et al., 2015; Amann et al., 2020; Buckingham et al., 2022). Field trials are in their nascent stages, and monitoring, reporting, and verifying (MRV) carbon dioxide removal in open, heterogeneous, and multiphase soil systems face inherent challenges (Clarkson et al., 2023), although recent efforts have started to address them (Amann & Hartmann, 2022; Reershemius et al., 2023; Knapp et al., 2023). Specifically, soil-based mass balance approaches, initially used for natural chemical weathering but modified to reduce analytical error, could be a promising option to resolve the small signal-to-noise ratios in EW mineral cation depletion (Reershemius et al., 2023). When EW is applied to significant portions of a watershed area, stream water chemistry analyses may also be beneficial to understand the transport of the mineral dissolution products (Larkin et al., 2022), as in the case of agricultural liming (Hamilton et al., 2007). Quantifying this transport from the field to CO_2 storage locations, such as deep aquifers or the oceans, is a crucial and yet largely unexplored EW aspect (Hartmann et al., 2013; Zhang et al., 2022; Bertagni & Porporato, 2022; Calabrese et al., 2022).

Within this intricate context, current estimates of EW potential as a NET heavily rely on models, mostly vertically explicit reactive transport models, where minerals added to the topsoil layers undergo dissolution based on transition state theory (Taylor et al., 2016; Beerling et al., 2020; Kantzas et al., 2022; Baek et al., 2023). While these models could comprehensively treat reacting chemical species across a heterogeneous soil profile, they are usually used under simplifying assumptions, such as constant vertical water flow and homogeneous soil properties. An alternative, spatially lumped approach focuses on the temporal dynamics of average quantities within the upper soil layers – the most dynamic soil layers, where ground rocks are introduced – hence emphasizing temporal over spatial variability (Cipolla et al., 2021a, 2021b). Given the direct and indirect impacts of hydroclimate conditions and soil moisture dynamics on weathering rates, capturing temporal variability is crucial. Soil moisture influences the surface area of EW material in contact with water and the dilution and leaching of weathering products. Moreover, it affects biotic and abiotic soil processes influencing EW dynamics, including carbon cycling, bacterial activity, and solute, heat, and gas transfers (Manzoni et al., 2012; Miele et al., 2023; Porporato & Yin, 2022).

Surprisingly, despite numerous experimental works in the last decade (Dietzen et al., 2018; te Pas et al., 2023; Kelland et al., 2020; Amann et al., 2020; Renforth et al., 2015; Vienne et al., 2022; Buckingham et al., 2022), comparisons of model results with experimental observations have been minimal (Kelland et al., 2020). An extensive model-data comparison is hence pivotal, not only to validate EW models for realistic assessments of net-zero scenarios (Kantzas et al., 2022; Buckingham et al., 2022), but also to improve modeling assumptions, provide a hypothesis-testing tool to investigate EW processes, design better experiments, and quantify uncertainty.

Our work addresses this gap, advancing an ecohydrological and biogeochemical model for EW dynamics in the upper soil layers and presenting an extensive and systematic model-experiment comparison. Specifically, the model is an evolution of the model originally developed by (Cipolla et al., 2021a), including several improvements in model closures and adding new model components (Sec. 2). The model performance is then compared with four experimental datasets covering a gradient of complexity, from simple closed incubation systems to more complicated, open mesocosm experiments (Sec. 3). The model-data comparison demonstrates that the model captures the dynamics of the primary variables of interest and provides crucial insights into weathering rates (Sec. 4). We finally identify model limitations and discuss areas requiring further theoretical and experimental exploration.
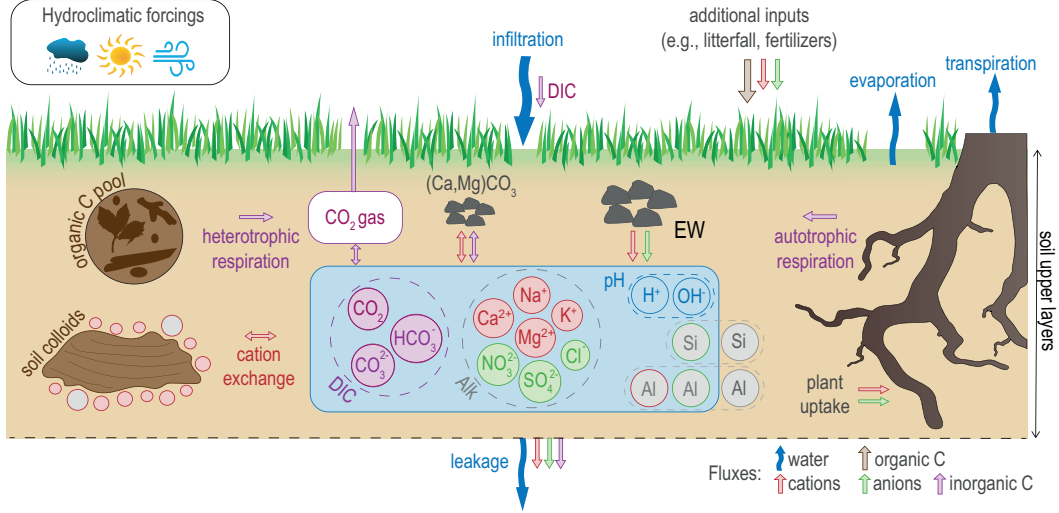
Figure 1. Sketch of the biogeochemical and ecohydrological processes represented in the model.

2 EW Model for the Upper Soil Layers

This model builds upon prior work on EW in the topsoil layers (Cipolla et al., 2021a, 2021b) incorporating several extensions and improvements in model closures and new model components. The model emphasizes the dynamic behavior of depth-averaged quantities within the root zone. The depth-averaged approach is especially appropriate when agricultural practices like mixing the ground rock have homogenized the upper soil layers (Porporato & Yin, 2022). The critical components of the model revolve around the intricate interplay between the water balance, influenced by stochastic infiltration rates, and the biogeochemical processes occurring within the multiphase soil porous media. Fig. 1 provides an overview of the main model components. In this section, we discuss the mass balances for the key variables of interest, which form a dynamic system of ordinary differential equations (ODEs). Jointly with the ODE system, we solve a set of algebraic equations based on a quasi-steady-state approximation to account for aqueous carbon and aluminum speciation and the cation redistribution between adsorbed and dissolved phases (Appendix A). The dynamics of plants and their roles in EW are presented in Appendix B.

2.1 Hydroclimate and Moisture Dynamics

Hydroclimatic forcings such as temperature and rainfall exert critical controls on weathering rates (Calabrese & Porporato, 2020; Deng et al., 2022) by directly influencing water availability and distribution, mineral dissolution kinetics and impacting various biogeochemical processes, including biotic activity and chemical equilibria. In our modeling framework, these hydroclimatic factors can be introduced through observational or reanalysis data or generated through modeling for future projections. Of particular significance to the correct representations of weathering dynamics are the short-term hydrological fluctuations because of their nonlinear feedback on soil hydro-biogeochemistry (Laio et al., 2001b; Porporato, D'Odorico, et al., 2003; Cipolla et al., 2021a; Porporato & Yin, 2022; Dong et al., 2023). Consequently, our modeling framework incorporates a water mass balance reproducing the time (t) evolution of relative soil moisture (s) within the soil depth (Z)

$$nZ\frac{ds}{dt} = R(t) - Q(s,t) - E(s) - T(s) - L(s), \tag{1}$$

where n is soil porosity, $R(t)$ is rainfall, $Q(s,t)$ is runoff, $E(s)$ is evaporation, $T(s)$ is plant transpiration, and $L(s)$ is leakage. In the absence of data, rainfall can be modeled as a stochastic marked Poisson process (Rodríguez-Iturbe et al., 1999; Porporato & Yin, 2022). Surface runoff, resembling Horton overland flow, is activated when the rainfall exceeds the available storage capacity. Evaporation and transpiration fluxes are influenced by soil moisture and vegetation cover (Laio et al., 2001a), and their cumulative effect is bounded by the potential evapotranspiration (ET_0), which is estimated using the Penman-Monteith method for a reference crop based on climatic conditions such as temperature, wind speed, latitude, and albedo (Allen et al., 1998). Water leakages to lower soil horizons are modeled as a power law of soil moisture with coefficients depending on soil texture (Laio et al., 2001b).

2.2 Organic Carbon and Heterotrophic Respiration

In the topsoil layers, soil carbon exists in organic and inorganic forms. The flux from organic to inorganic carbon pools results from the decomposition of soil organic matter, mostly driven by biotic processes like bacterial activity. This flux, called heterotrophic soil respiration, is a key contributor to elevated CO_2 levels in soil air, making it a critical factor in the potential EW efficiency in soil carbon sequestration. To model the dynamics of organic carbon (OC), here considered as dead biotic material, we employ a simple balance that includes an addition term (ADD), accounting for inputs like litterfall or soil amendments, and a decomposition term (DEC) representing biotic activity (Porporato, D'Odorico, et al., 2003; Cipolla et al., 2021a). The mass balance for OC is

$$\frac{d\text{OC}}{dt} = \text{ADD} - \text{DEC}. \tag{2}$$

Depending on the available information, the addition of OC can be assumed to be constant, vary seasonally, or be based on photosynthetic activity. The decomposition term is proportional to the available OC through a moisture- and temperature-dependent coefficient (Porporato, D'Odorico, et al., 2003; Cipolla et al., 2021a). A fraction r of the decomposed OC is converted into inorganic carbon, defining soil heterotrophic respiration ($\text{RESP}_h = r\,\text{DEC}$). The remaining fraction $(1 - r)$ is assumed to be converted into living biomass of soil biota (e.g., bacteria, fungi, and soil fauna), which is not explicitly modeled (Porporato, Laio, et al., 2003). While here we use a minimalist soil OC model, more elaborate representations of the OC cycle (e.g., with explicit microbial dynamics) may be adopted (Wieder et al., 2013; Jha et al., 2023) based on specific scientific questions being addressed in the interactions between OC and EW.

2.3 Inorganic Carbon Pools

EW negative-emission potential hinges on the sequestration of inorganic carbon, mainly in the form of aqueous carbonates within soil water and throughout the hydrological cycle, or through the formation of secondary carbonate minerals, albeit with a 50% reduction in CO_2 removal efficiency (Hartmann et al., 2013; Bertagni & Porporato, 2022). The main components of soil inorganic carbon include CO_2 in the soil air phase, dissolved inorganic carbon (DIC) in the soil water, and carbon stored in mineral forms. Given that the equilibration timescale of aqueous and gaseous forms is much faster than that of carbonate mineral precipitation and dissolution, we consider two distinct inorganic carbon pools: one that combines aqueous and gaseous forms (IC) and another accounting for mineral inorganic carbon (MIC). The overall mass balances for IC and MIC are expressed as:

$$\frac{d\text{IC}}{dt} = \text{RESP}_{h+a} + I_w \cdot [\text{DIC}]_{I_w} - L \cdot [\text{DIC}] - F_{\text{ADV+DIFF}} + W_{\text{(Ca, Mg)CO}_3}, \tag{3}$$

$$\frac{d\text{MIC}}{dt} = -W_{\text{(Ca, Mg)CO}_3}, \tag{4}$$

where $[\cdot]$ indicates concentration. $\text{RESP}_{\text{h+a}}$ is the sum of heterotrophic and autotrophic respiration, respectively. Autotrophic respiration (RESP_{a}), namely the release of CO_2 gas by plant roots, is estimated to scale with vegetation (Appendix B) and to be equivalent to heterotrophic respiration (Sec. 2.2) when plants are fully grown (Bond-Lamberty et al., 2004). Another minor source of inorganic carbon in the soil is the DIC in infiltrating water ($I_w = R - Q$). IC can exit the control volume as aqueous DIC through leaching ($L \cdot [\text{DIC}]$) or as gaseous CO_2 to the atmosphere through diffusive or advective fluxes ($F_{\text{ADV+DIFF}}$) (Cipolla et al., 2021a). The term $W_{(\text{Ca, Mg})\text{CO}_3}$ accounts for the dissolution (> 0) or precipitation (< 0) of calcium and magnesium carbonates, modeled following (Kirk et al., 2015). The redistribution of IC between soil air CO_2 and aqueous carbonates follows equilibrium assumptions (Appendix A).

2.4 Biogeochemistry of Alkaline and Acid Elements

To promote inorganic carbon sequestration, EW aims to release alkaline cations (Ca^{2+}, Mg^{2+}, K^+, Na^+) in soil water and throughout the hydrological cycle (Hartmann et al., 2013). These cations increase water alkalinity and promote a transfer of CO_2 from the atmosphere to the water by forming aqueous carbonates in favorable water-chemistry conditions (Bertagni & Porporato, 2022). We hence consider four mass balances for each of these alkaline cations, indicated generically as X. The mass balances for any total cation content (X_{tot}) within the control volume, comprising cations dissolved in the soil solution and those adsorbed onto soil colloids, can be written as

$$\frac{d\text{X}_{\text{tot}}}{dt} = I_{\text{X}} + \text{EW}_{\text{X}} + W_{\text{XCO}_3} - (L+T)[\text{X}] - \text{UP}_{\text{X}}. \tag{5}$$

I_{X} accounts for background cation inputs like litterfall decomposition, fertilizer addition, and background weathering processes. EW_{X} denotes the cation release by the EW application, and W_{XCO3} is the release from the weathering of Ca or Mg carbonate. The term $(L+T)[\text{X}]$ characterizes the outflow resulting from leaching and plant passive uptake, while UP_{X} pertains to active plant uptake during growth (Appendix B). Given the total cation amount in the control volume, the partitioning between adsorbed and aqueous components follows equilibrium assumptions (Appendix A).

A similar mass balance approach applies to the major strong anions commonly found in soil solutions (e.g., Cl^-, NO_3^{2-}, SO_4^{2-}). Conveniently, we do not need to discriminate between the various anions of the strong acids because i) EW aims to increase cation concentrations, ii) anion adsorption is mostly negligible in many soil environments, iii) it is the cumulative presence of these anions that defines soil water alkalinity (Appendix A). We can thus collectively denote these anions as An and write a single mass balance

$$\frac{d\text{An}_{\text{tot}}}{dt} = I_{\text{An}} - (L+T)[\text{An}], \tag{6}$$

where I_{An} signifies background anion input, and $(L+T)[\text{An}]$ represents anion losses due to leakages and passive plant uptake.

2.5 Silicon and Aluminum Balances

Since the most promising options for large-scale EW applications are silicate minerals and rocks, EW is anticipated to release large amounts of silicon (Si) into soils. This constitutes a potential EW co-benefit, as soil Si is a biotic nutrient that enhances plant immune system (Fauteux et al., 2005; Kim et al., 2014). Soil Si chemistry is rather complex, comprising dissolved species, amorphous solid phases, and organic and inorganic complexes (Schaller et al., 2021), and its dynamics is expected to impact soil formation processes on long timescales (Weil & Brady, 2016). Given that Si impact on the CO_2 sequestration dynamics by EW is minor, here we follow a simplified approach, wherein we consider Si as dissolved silicic acid. More complex mass balances could be adopted

depending on the goal of the investigation. The mass balance hence is

$$\frac{d\text{Si}_{\text{tot}}}{dt} = I_{\text{Si}} + \text{EW}_{\text{Si}} - (L + T)[\text{Si}] - \text{UP}_{\text{Si}}, \tag{7}$$

where I_{Si} represents background Si inputs, EW_{Si} accounts for Si released through EW
applications, $(L+T)[\text{Si}]$ signifies Si outflow due to leaching and passive plant uptake,
and UP_{Si} denotes active plant uptake during growth.

Aluminum is a prevalent element in highly weathered, acidic soils, where it can be
found in complexes, in the soil solution, or as cations adsorbed into soil colloids. In acidic
conditions, aluminum plays a crucial role as a buffering agent but can be toxic to soil
biotic activity and plants in high concentrations (Weil & Brady, 2016). Although Al is
an undesired product, EW applications may release some of it, depending on the min-
eral composition of the rock applied. The mass balance for aluminum is expressed as

$$\frac{d\text{Al}_{\text{tot}}}{dt} = I_{\text{Al}} + \text{EW}_{\text{Al}} - L[\text{Al}_{\text{mob}}], \tag{8}$$

where I_{Al} and EW_{Al} correspond to background and EW-induced Al releases, respectively.
Aluminum losses are assumed to occur solely through the leaching of Al's more soluble
and mobile forms ($[\text{Al}_{\text{mob}}]$), which can be abundant in highly acidic (pH< 4.5) or al-
kaline (pH> 7) conditions. Aluminum speciation reactions are reported in Appendix
A.

2.6 Rock Weathering

Modeling rock weathering is pivotal to understanding and quantifying EW dynam-
ics and temporal efficiency. Applied rocks are typically composed of various minerals,
and the release of a specific element like an alkaline cation X (Sec.2.4) results from the
collective contribution of mineral dissolution. This contribution depends on the mineral
dissolution rate (W_i) and the mineral surface area (SA_i), and can be expressed as

$$\text{EW}_{\text{X}} = \sum_i m_{\text{X},i} \cdot \text{SA}_i \cdot W_i(s, \Theta, \text{pH}) \tag{9}$$

where $m_{\text{X},i}$ accounts for the stoichiometry of the element X in the mineral i, and Θ stays
for temperature. The same equations, with coefficients $m_{\text{Al},i}$ and $m_{\text{Si},i}$, apply to the re-
lease of Al and Si, namely EW_{Al} and EW_{Si} in eqs.(7) and (8). The mineral surface area
SA_i is determined according to the methodology proposed by Beerling et al. (2020), which
accounts for the dynamically evolving rock composition and particle distribution and the
fractal dimension of the particle surface.

For the weathering rates, we follow previous EW modeling efforts (Taylor et al.,
2016; Beerling et al., 2020; Kantzas et al., 2022) and use the semi-empirical formula by
Palandri (2004). This seminal formulation, originally developed in the work of Lasaga
(1984), is based on dissolution experiments in stirred reactors without diffusive limita-
tions and under conditions far from equilibrium. The formula accounts for the most well-
studied mechanisms of mineral dissolution, driven by the water species H_2O, H^+, and
OH^-. As previously implemented by Cipolla et al. (2021a), we also consider the depen-
dence of mineral dissolution rates on the relative soil moisture value (s) to account for
the wet portion of the mineral surface that can actually undergo dissolution. The for-
mula for the weathering rate of each mineral can thus be expressed as:

$$W_i = F_D \cdot s \cdot \sum_j k_{i,j}(\Theta) \cdot a_j^{n_{i,j}} \cdot (1 - \Omega_i^{p_{i,j}})^{q_{i,j}}, \tag{10}$$

where j is the individual weathering agent (H_2O, H^+, OH^-) and a_j are the agent ac-
tivities (here approximated as concentrations). $k_{i,j}(\Theta)$ are the mineral- and agent-dependent
rates accounting for temperature (Θ) effects, and $n_{i,j}$ are the reaction order constants

(Palandri, 2004). Ω_i is the mineral saturation index (Morel et al., 1993). The coefficients $p_{i,j}$ and $q_{i,j}$ have been quantified only for very few minerals and agents and are approximated to unity (Palandri, 2004). F_D is a dissolution factor that we will quantify based on experimental observations. As later discussed (Sec. 4.1), the observation-driven quantification of F_D is crucial to assess actual weathering rates and the validity of Palandri's formulation in the soil environment.

2.7 Model Setup and Simulation Example

The EW model requires a characterization of the hydroclimatic forcings, the EW material and application rate, the plant, and the soil biophysical properties. Rainfall and temperature are key hydroclimatic forcings that impact virtually all model components. Wind speed and albedo play a role in influencing potential evapotranspiration (Allen et al., 1998). For EW application, details include the amount and mineral composition of the applied rock, particle size distribution, and specific surface area. Plant characterization involves parameters like carrying capacity, growth rate, and root area index, measured or derived from the literature (Appendix B). Soil characterization requires details on soil texture, initial organic carbon content and pH, and inorganic chemistry. Notably, assuming a quasi-steady state equilibrium of the soil chemistry allows constraining the air-water carbonate system using a single quantity (e.g., the CO_2 partial pressure) in addition to the soil pH (Stumm & Morgan, 1996). For the biogeochemistry of the major ions, minimum initial data requires either the adsorbed fractions on the cation exchange capacity (CEC), the concentrations in the soil solution, or the total quantities per unit of soil. The others are determined through the Gaines-Thomas convention (Appendix A). In the absence of specific data, background elemental input fluxes, e.g., I_X in eq. (5), can be defined to balance background losses, e.g., $[x]_{initial}(\overline{T}+\overline{L})$ where the bar denotes temporal averaging. This approach ensures that the initial condition represents a long-term average state of the soil that is reestablished whenever the EW application is absent or concluded.

Fig. 2 shows an example of a 1-year simulation for a 1 kg/m^2 (10 tonn/ha) EW application with forsterite (Mg_2SiO_4) in a temperate humid climate (10-year results are reported in Fig. S1). The mean temperature is 13°C, and the yearly cumulative rainfall is 1200 mm. The simulated soil is an organic-rich (initial OC is 5%) and acidic (initial pH is 4) loam. Results show how the low soil pH favors the mineral dissolution rate but impedes the formation of bicarbonate in the soil solution (Bertagni & Porporato, 2022; Dietzen & Rosing, 2023). The trend reverses when the pH gets around 6, with slower dissolution rates and bicarbonate formation. The CEC base saturation increases as the pH rises, and Mg^{2+} and Ca^+ replace the acid ions H^+ and Al^{3+}, showing the potential of EW for liming purposes.

3 Comparison with Experiments

This section compares our model outcomes with available experimental data. Specifically, we use four different experimental datasets derived from experiments conducted at varying levels of complexity: i) small-scale vials open to the atmosphere and with moist acidic soils (Dietzen et al., 2018); ii) small down-flow soil columns open to the atmosphere and water leaching (te Pas et al., 2023); iii) two more complete mesocosm experiments incorporating growing vegetation (Kelland et al., 2020; Amann et al., 2020). The comparison with these different experimental setups gives the advantages of compartmental investigations of the model performance and a broad examination of EW dynamics under different environmental forcings. Because our model is spatially lumped and designed for the upper soil layers, we could not include in the analysis experiments focusing on EW in vertically deep and heterogeneous soil cores (Renforth et al., 2015; Vienne et al., 2022; Buckingham et al., 2022).
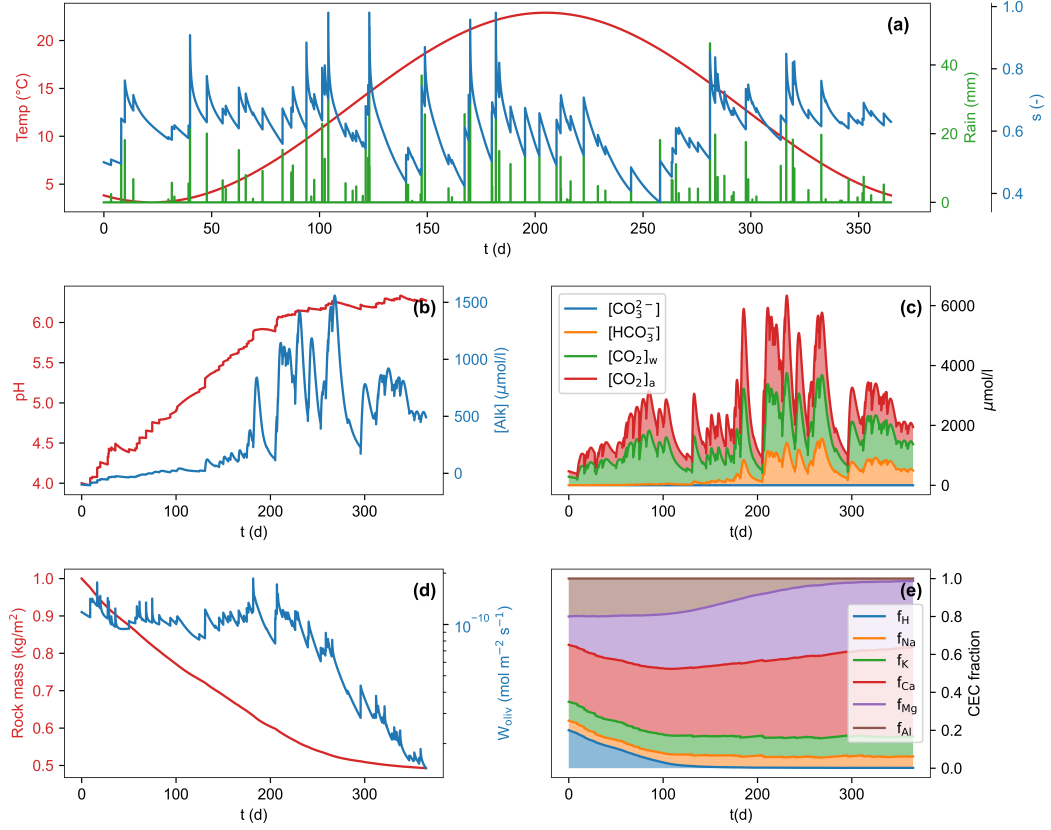
Figure 2. Example of model output for an EW application (1 kg/m^2) with forsterite (Mg$_2$SiO$_4$) in a temperate humid climate. (a) Temperature, rainfall, and soil moisture. (b) Soil water pH and alkalinity. (c) Inorganic carbon speciation. (d) Mineral mass and weathering rate. (e) Soil cation adsorption. See Fig. S1 for the results extended to 10 years.
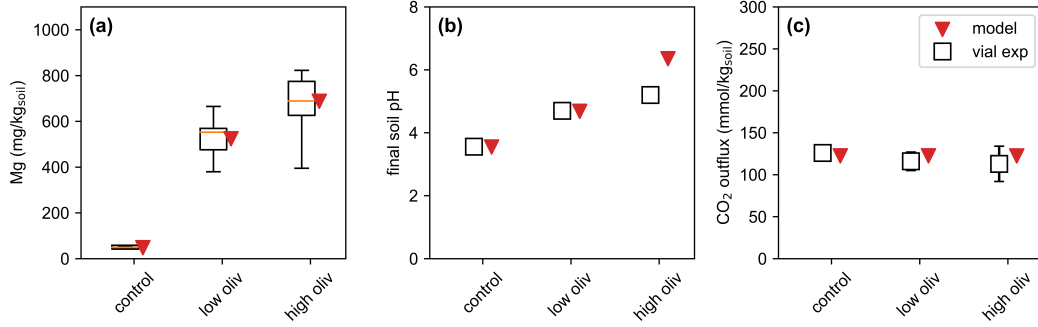
Figure 3. Model-experiment comparison based on the vial experiments by Dietzen et al. (2018). (a) Final Mg accumulation in the soil. For the experimental replicates (10 for each case), the central line represents the median value, the boxes span from the 25th to 75th percentiles, and the whiskers extend from the minimum to the maximum value. (b) Final soil pH (c) Mean cumulative net CO_2 flux to the atmosphere, showing minimal variations across treatments. Error bars indicate experimental standard deviation (SD) – not shown if shorter than the symbol size.

3.1 Acidic Soil in Vials

Our first comparison involves the experiments by Dietzen et al. (2018), which entailed a three-month soil incubation study to assess the weathering of olivine (mainly composed of forsterite, Mg_2SiO_4) and its impact on available Mg levels, pH, and soil CO_2 flux. The experiments employed 110 ml open vials filled with soil that remained consistently moist throughout the study. Olivine was added at varying application rates. The open vials allowed CO_2 exchange with the atmosphere while preventing downstream water leaching. Although these experiments simplified the soil environment considerably, they provided valuable insights by enabling a direct assessment of the soil-water-air chemistry influenced by the mineral dissolution.

We conducted model simulations, configuring the numerical parameters to align with the experimental conditions. The sandy soil was characterized by high acidity (initial pH = 3.55) and substantial organic carbon content (initial OC = 5.5%). Olivine powder with an average diameter of 20 μm was applied at two distinct rates, equivalent to 1 and 5 kg/m^2. The soil was constantly moist, and the temperature was fixed at the experimental value of 22 °C. The initial CO_2 concentration in the soil air was set at 23 times atmospheric values to reproduce the observed soil respiration flux. Data about adsorbed species were not provided in the experimental work, so we estimated a CEC of 10 cmol$_c$/kg$_{soil}$ with 10% base saturation from literature values for extremely acidic sandy loam (Weil & Brady, 2016). The simulations encompass the three experimental scenarios: control and low and high olivine applications.

The comparison between simulations and experiments is presented in Fig. 3, which highlights the Mg accumulation in the vial due to mineral dissolution (a), the soil pH shifts (b), and the flux of CO_2 from the soil to the atmosphere (c). The simulations closely align with the experimental findings in all three scenarios. Notably, the Mg accumulations in the vials constrain the weathering rates since there are no Mg losses from the control volume. As further commented in the discussion (Sec. 4.1), the dissolution factor F_D in the weathering formula (10) had to be adjusted to values $\mathcal{O}(0.1)$, implying that Palandri's formula (10) overestimated the mineral dissolution rate. The pH shifts show good agreement except in the high-olivine application, suggesting that experimental soil pH is more buffered than what our numerical simulations reproduce. The CO_2 flux to
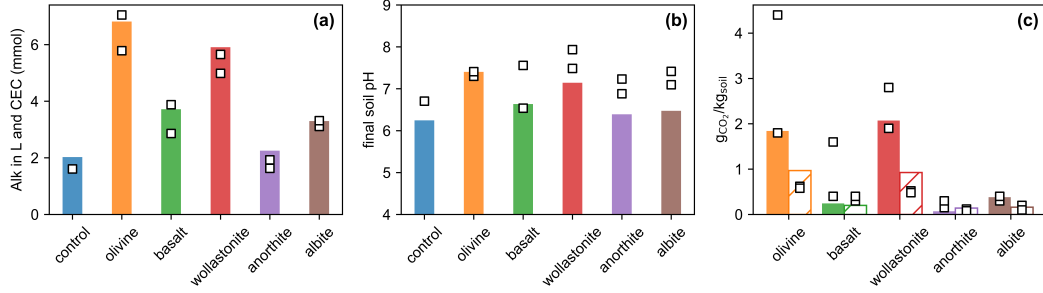
Figure 4. Model-experiment comparison based on the down-flow bottle experiments by te Pas et al. (2023). Square symbols stay for the experimental replicates. (a) Total alkalinity observed in the leaching and on the cation exchange capacity. (b) Final soil pH. (c) Potential (filled bars) and effective (dashed bars) CO_2 sequestration.

the atmosphere remains nearly identical in the control and olivine treatments, implying no CO_2 sequestration in either experiment or model. This is due to the low pH levels that impede aqueous carbonate formation (Bertagni & Porporato, 2022; Dietzen & Rosing, 2023). More extended experiments allowing for further olivine dissolution would raise the pH to favorable values for CO_2 sequestration.

3.2 Soil Columns with Leaching

Our second comparison is with experiments conducted by te Pas et al. (2023), featuring small down-flow soil columns of 180 ml polyethylene containers. These columns were equipped with perforated bases to enable water leaching. The experiments thus account for a rudimentary hydrologic cycle, wherein the soil-rock mixture undergoes wet-dry cycles with water added every three days. A further advantage of these nine-week experiments is that they assessed the enhanced weathering potential of five distinct rocks and minerals: forsterite (Mg_2SiO_4), wollastonite ($CaSiO_3$), anorthite ($CaAl_2Si_2O_8$), albite ($NaAlSiO_3$), and basalt.

We conducted model simulations utilizing parameters directly derived from the experiments. The sandy soil had an initial pH of 5.2 and an organic carbon content of 2.1%. Deterministic rainfall events of constant intensity were applied at three-day intervals. The resulting rainfall regime (around 3200 mm/yr) is typical of tropical regions. Rock powder application mirrored the experimental high load of 12.5 kg/m² across all cases, incorporating different particle size distributions and specific surface areas. Albite mineral composition included a 3% of wollastonite. Without data regarding the mineral composition of basalt, we adopted the basalt characterization from Beerling et al. (2020). The temperature was set at 22 °C. Equilibrium-based initial conditions for adsorbed and dissolved species were established based on experimental measurements of total alkaline cation (Ca, Mg, K, Na) quantities. The CEC was fixed at the effective CEC value (3 $cmol_c/kg_{soil}$) observed at the beginning of the experiments.

Figure 4 presents the model-experiment comparisons for the total alkalinity release by mineral dissolution (a), the increase in soil pH (b), and the CO_2 captured by the EW applications (c). The total alkalinity release includes alkalinity observed in leaching and soil adsorption (see Fig. S2 for the partitioning between the two phases) and constrains the mineral weathering rates, giving F_D values in the weathering formula (10) consistently below one. The pH shifts show a reasonable agreement, although the numerical simulations do not fully reproduce the increase in pH that is observed experimentally. This is not surprising since the model does not explain the increase in soil pH that is ob-

served in the experimental setup without rock application. The pH temporal dynamics (Fig. S2) further reveal a model-experiment difference in the first days of the experiment, where the model does not reproduce the pH experimental drop likely driven by the acidity released by the cation exchange. Following the experimental work (te Pas et al., 2023), we quantified the CO_2 sequestration in two ways: one based on the alkalinity liberated through rock dissolution (potential CO_2 sequestration) and the other accounting for aqueous carbonate leaching and additional inorganic carbon stored in the soil (effective CO_2 capture). Consistently with the experiments, the effective approach yielded significantly lower estimates than the potential method because a portion of the alkalinity liberated by the mineral dissolution is adsorbed into soil colloids, not promoting carbonate formation.

3.3 Mesocosms with Vegetation

The third and fourth comparisons are with mesocosm experiments (Kelland et al., 2020; Amann et al., 2020). A distinctive feature of these experiments was the inclusion of actively growing vegetation, specifically sorghum in Kelland et al. (2020) and wheat and barley in Amann et al. (2020). Vegetation introduces complexities to soil hydrology and biogeochemistry through water transpiration, nutrient uptake, and CO_2 autotrophic respiration (Appendix B). Although the representation of the hydrological cycle in these experiments remained somewhat simplified with periodic (1-7 days) and fixed amounts of water addition, the dynamic interplay with vegetation growth resulted in notable water flux shifts during the growing season. This allowed for an expanded comparative analysis, including examining hydrological and soil biogeochemical processes.

3.3.1 Reactor Columns

Kelland et al. (2020) conducted experiments in reactor columns measuring 16 cm in diameter and 50 cm in depth over 120 days. We ran model simulations based on the experimentally observed parameters as in the previous comparisons. The soil was classified as a clay loam with an initial pH of 6.6 and an organic carbon content of 1.2%. The simulations incorporated a rainfall regime typical of temperate humid and tropical regions (about 2000 mm/yr), with water added every five days. To estimate the potential evapotranspiration, we numerically recreated the experimental artificial day. This involved maintaining photosynthetically active radiation (800 μmol photons m^{-2} s^{-1}) for 18 hr during the initial 60 days and 10 hr for the subsequent 60 days. Daily temperatures were computed by temporally averaging the 25 and 17 °C of the artificial day and night, respectively. We used experimental values for the basalt application (high load of 10 kg/m^2), rock mineral composition, specific surface area, and particle size distribution. Due to the depth-averaged model framework, we could not reproduce the experimental vertical heterogeneity, with basal being mixed only in the first 25 cm of the soil column. The CEC was fixed at the experimental value of 25 cmol$_c$/kg$_{soil}$, and the initial saturation fractions were estimated based on the cation concentrations measured in the leachate of the untreated experiment.

Fig. 5 presents the model-experiment comparison for the elemental release through basalt dissolution (a), the impact on soil pH (b), and potential and effective CO_2 sequestration (c). The model well captures the release of alkaline nutrients Ca, Mg, and K. We stress, however, that the very fast dissolution of apatite, $Ca_5(PO_4)_3(OH)$, comprising around 3% of the basalt, could not be numerically reproduced (see the discussion section) and has been added at *a posteriori* to the simulation results. The model instead overestimates the release of Na and Si, suggesting that plants and fungi in the experiments might have driven incongruent dissolution reactions. It might also be that the Si experimental values are biased low due to underestimation of the Si pool by extraction with ammonium acetate (Wang et al., 2004). There is also a promising model-experiment agreement in the Ca, Mg, and Si partitioning among soil, plant, and leachate (Fig. S3).
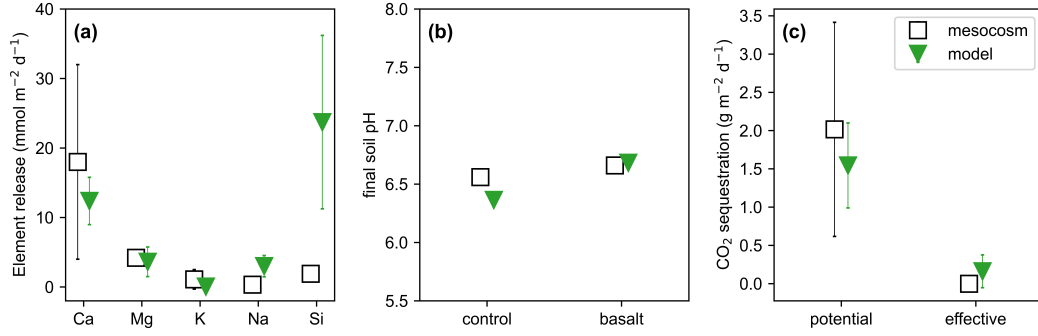
Figure 5. Model-experiment comparison based on the mesocosm experiments by Kelland et al. (2020). (a) Daily averaged elemental release of basalt dissolution per land surface unit, with bars indicating ± 1 SD. (b) Final pH. (c) Potential (alkalinity release) and effective (aqueous carbonate leaching) CO_2 sequestration.

Moreover, the model effectively reproduces the potential CO_2 sequestration resulting from alkaline element release, demonstrating substantially higher values in both experiments and simulations than the effective CO_2 sequestered through aqueous carbonate leaching.

3.3.2 Rain Barrels

Amann et al. (2020) performed experiments in rain barrels measuring 46 cm in diameter and 26 cm in depth over a year. The soil was classified as loamy sand with an initial pH of 7 and an initial organic carbon content of 1.2%. The simulations mimic a rainfall regime of 800 mm/yr, with rainfall events distributed every day or week, with little difference in the results between the two cases. The particle size distributions differentiate between coarse and fine olivine (mostly forsterite, Mg_2SiO_4) applications of 22 kg/m^2, with 25 and 720 μm being the dominant diameter classes, respectively. The simulations assume that the olivine is mixed across the barrel, while, in the experiments, olivine was mixed in the top layer of approximately 11 cm. Temperature was varied with a sinusoidal function across the year, from a minimum of 6°C to a maximum of 25°C. The CEC was fixed at the experimental value of 8.6 cmol$_c$/kg$_{soil}$, initially saturated by 86.5% of Ca, 5% of Mg, 5% of K, 3% of Na, and 0.5% of H and Al (Amann et al., 2020). We ran six simulations for the control case and the coarse and fine olivine applications, with and without vegetation.

Fig. 6 presents the model-experiment comparisons in terms of hydrological balance (a), pH dynamics (b), soil air CO_2 (c), and CO_2 sequestration (d). For this experimental setup, leaching is a significative proxy for hydrologic partitioning since evapotranspiration directly results from the difference between water input and leaching. The simulations reproduce the leaching seasonal patterns due to temperature and vegetation impacts. The pH dynamics show a reasonable agreement, with an increase in the soil pH in time due to the olivine dissolution. Both simulation and experiments show how vegetation tends to reduce the pH by cation uptake and CO_2 respiration. The soil air CO_2 dynamics also show promising results, with the model reproducing seasonal variations and the influence of the vegetation in increasing the CO_2 concentration.

Regarding CO_2 sequestration, we estimated the potential CO_2 capture due to the Mg released by mineral dissolution and the effective CO_2 capture, here quantified through the Mg observed in the leached water, as done in the experimental work. Note that the
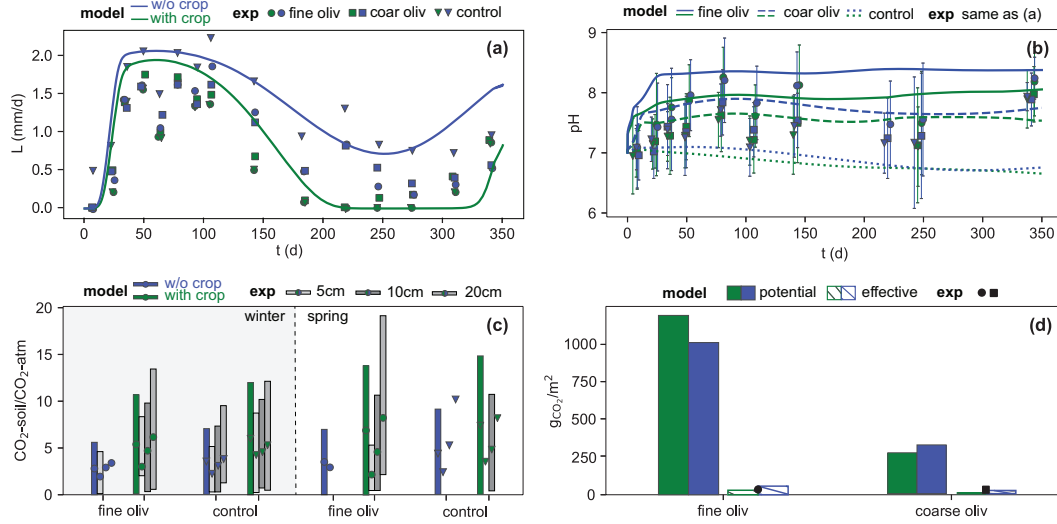
Figure 6. Model-experiment comparison based on the mesocosm experiments by Amann et al. (2020), in the presence (green) and absence (blue) of vegetation. (a) Leaching fluxes. (b) pH dynamics with error bars indicating ± 1SD. The reported experimental values are averages between shallow (1.5 cm) and deep (24 cm) measurements. (c) Soil air CO_2, showing experimental measurements obtained at different depths and depth-averaged model results. Bars indicate ± 1SD when available. For the numerical results, winter and spring are defined as the experiment's first and second 100 days, respectively. (d) Potential and effective CO_2 sequestration, with experimental results showcasing averaged effective CO_2 sequestration with and without vegetation.

experimental effective CO_2 capture has been reassessed from Mg leachate data due to a dimensional inconsistency in the formula (2) reported by Amann et al. (2020). The potential CO_2 capture is much higher than the effective one due to the loss of alkaline cations to soil adsorption and plant uptake. Interestingly, vegetation has a dual influence on CO_2 removal: plant uptake of alkaline cations reduces the effective CO_2 removal, but plant-induced soil acidification enhances the mineral dissolution rates, increasing the potential CO_2 removal. Consequently, our results suggest a trade-off in CO_2 removal efficiency, with plant-absent scenarios showcasing slower but more efficient removal processes. In contrast, plant-present scenarios feature faster but less efficient removal processes.

4 Discussion

The overall favorable agreement between model outcomes and experimental observations allows us to provide critical insights into the weathering rates. We then identify and discuss areas requiring further theoretical and experimental exploration.

4.1 Weathering Rates

The assessment of EW is intricately linked to the precise determination of rock weathering rates, whose parameters are surrounded by considerable uncertainty (Calabrese et al., 2022). The theoretical formulation used here (Palandri, 2004) is widely regarded as comprehensive and is commonly applied in EW assessments (Taylor et al., 2016; Beerling et al., 2020; Kantzas et al., 2022). However, this formulation is derived from experimental data from stirred reactors without diffusive limitations and under conditions far from equilibrium. In the complex, multiphase, and porous soil environment, numerous
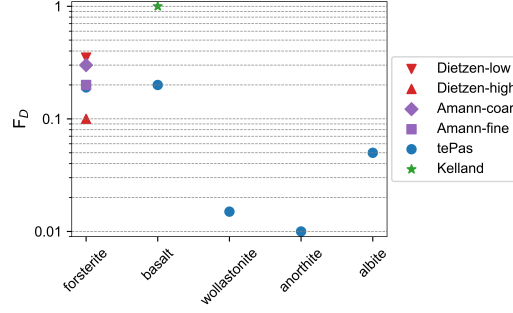
Figure 7. Dissolution factor (F_D) used in the weathering rate equation (10) to reproduce the experimental observations of alkalinity releases.

overlooked biotic and abiotic processes may influence dissolution rates: i) concentration gradient formation into the aqueous phase near mineral surfaces, ii) primary and secondary mineral coatings, iii) fungal and bacterial activity, iv) catalyzation or inhibition of the dissolution reactions due to the presence of other chemical species. While some specific processes are expected to promote dissolution (e.g., biotic activity), others predominantly impede it (e.g., particle coatings). As a result, the validity of the formula for EW applications remains an open question.

As indicated by our model-experiment comparison, Palandri's formulation requires a correction with a dissolution factor, F_D in (10), which is consistently below one for most experimental setups and rocks (Fig. 7). In other words, minerals and rocks dissolve slower than conventionally assumed. While these findings align with the acknowledgment that *Actual equilibration rates are expected to be much slower than those predicted by the selected computer code* (Palandri, 2004), they carry significant implications. Specifically, the results underscore the need to refine weathering formulations from both a process and data perspective, systematically incorporating other soil biotic and abiotic processes that influence weathering. They also highlight that unless field weathering rates prove to be much higher than what is observed in small-scale experiments, considering only the biotic-driven enhancement of weathering rates (namely $F_D > 1$) may lead to a significant overestimation of EW CO_2 removal potential (Beerling et al., 2020; Kantzas et al., 2022).

4.2 Limitations and Outlook

The model-experiment comparison presented in this study is only a first step in the direction of having robust assessments of EW models to reproduce observations across scales. Many advances will be needed from both modeling and experimental perspectives.

From a modeling point of view, the model presented here accounts for the primary variables of interest to assess the fate of the alkaline cations released by the EW applications and their corresponding inorganic carbon sequestration potential. It does not include feedback that the rock powder application may have on some soil physical and biotic processes. The different leaching fluxes observed in the experiments by (Amann et al., 2020) suggest that the rock powder impacts the soil texture and hydraulic conductivity, hence the soil water partitioning. Specific experiments evaluating the temporal evolution of soil physical properties are needed to incorporate such feedback in models, even though some theoretical estimates may be derived based on soil physics models (Jury & Horton, 2004). Furthermore, rock applications may influence biotic activity and the organic carbon balance, with potentially detrimental effects in tropical soils and peat-

lands (Klemme et al., 2022). Modeling advances could also include mass balances for heavy metal accumulations, such as nickel and copper, which are significant concerns in the context of EW applications (Haque et al., 2020; Dupla et al., 2023)

Compared to the more used reactive transport models, our model is simpler, not accounting for soil vertical heterogeneity and including fewer chemical species. This simplicity comes at the cost of spatial information but at the advantage of accessibility and a more concentrated examination of temporal dynamics. Interestingly, our model did not necessitate a semi-empirical pH buffer function commonly employed in EW simulations with reactive transport models to avoid unrealistic spikes in soil pH. This is intriguing since our buffering mechanisms incorporate only carbonate chemistry and cation adsorption while neglecting others like organic alkalinity. We attribute this success to implementing shorter simulation time steps, operating in the order of minutes rather than days, as seen in traditional reactive transport models. Nonetheless, our model encounters limitations in reproducing the rapid dissolution of certain minerals and materials (e.g., $Ca_5(PO_4)_3(OH)$ or $Ca(OH)_2$) due to pronounced spikes in alkalinity that hinder the numerical convergence of the implicit system (Appendix A). Looking ahead, a promising avenue involves integrating our model results with both reactive transport models and observational data to gain comprehensive insights into soil EW dynamics.

From an observational standpoint, it is worth acknowledging the temporal constraint within the available datasets. Specifically, only one of the experimental datasets used within this study spans a complete year (Amann et al., 2020), while others have a relatively shorter duration of a few months. Given the potential yearly timescales associated with the dissolution of EW rock powder, extrapolating results becomes challenging, especially considering that weathering rates may decrease over the years (Calabrese et al., 2022). Additionally, most experiments relied on elevated rock loadings (i.e., ≥ 10 kg/m^2) to enhance signals within the short experimental time frame, although such loadings may not be realistic for practical applications. There is also an opportunity to explore the influence of realistic stochastic rainfall regimes, which is often absent in current experimental setups. Integrating field observations of large-scale EW applications will hopefully address some of these temporal and loading limitations, offering insights into the compatibility between model results, small-scale experiments, and the practical considerations of large-scale field trials.

5 Conclusions

While enhanced weathering (EW) holds great promise as a negative emission strategy, thanks to its significant CDR potential, low technological prerequisites, and valuable co-benefits, no model has been shown to reproduce EW observations at scale. This deficit restricts our ability to make accurate quantitative predictions for assessments of CDR via EW. In this study, we took a benchmark step in this direction, advancing a relatively accessible ecohydrological and biogeochemical model whose results could be meticulously compared with four distinct experimental datasets of different complexity.

The model-experiment comparison demonstrates an overall favorable agreement for the primary variables of interest, including alkalinity release, pH dynamics, and CO_2 sequestration. The comparison also demonstrates that weathering rates are lower than traditionally assumed by one or two orders of magnitudes and highlights further research directions to improve our understanding and quantitative predictive power for EW as a NET. Finally, while representing EW dynamics within the soil's upper layers is crucial, EW negative emission potential is linked to the fate of rock dissolution products from the field to the ocean, a journey yet to be fully disclosed.

Appendix A Implicit System of Equilibrium Equations

We here report the implicit system of equilibrium equations solved under the quasi-steady approximation jointly with the system of ODEs (1)-(8). These equations are all coupled and quantify how total quantities within the control volume are distributed among the different soil phases. Specifically, alkaline cations (X_{tot}) are distributed between dissolved and adsorbed phases, inorganic carbon (IC_{tot}) is distributed between aqueous and air phases, and aluminum (Al_{tot}) exists dissolved in water, adsorbed to the soil matrix or in complexes with organic or inorganic matter. In formula

$$X_{tot} = nZs[X] + f_X CEC/n_X, \tag{A1}$$

$$IC_{tot} = nZs[DIC] + nZ_r(1-s)[CO_2]_a, \tag{A2}$$

$$Al_{tot} = nZs[Al]_{mob} + f_{Al}CEC/3 + Al_{imm}, \tag{A3}$$

where n_X is the cation valence and CEC is the cation exchange capacity. The latter indicates the moles of dissolved cations that can be adsorbed on soil colloids due to their negatively charged surface (Weil & Brady, 2016).

Cation Partitioning and Soil Adsorption. The master variable connecting alkaline cations and carbonate system is alkalinity (Alk). Expressed in terms of species that are conservative to changes in pH, temperature, and pressure (Wolf-Gladrow et al., 2007; Bertagni & Porporato, 2022), alkalinity is

$$[Alk] = 2[Ca^{2+}] + 2[Mg^{2+}] + [K^{2+}] + [Na^{2+}] - [An], \tag{A4}$$

where [An] indicates the cumulative concentration of the anions of the strong acids. Quantifying the dissolved cations in the soil solution requires assessing the cation partitioning between the dissolved and adsorbed phases. This is done using the Gaines-Thomas convention (Bleam, 2017). Specifically, five equations are used to describe the binary exchange of Ca^{2+} with Al^{3+}, Mg^{2+}, Na^+, K^+, and H^+:

$$\frac{f_{Ca}^3}{f_{Al}^2} = K_{Ca-Al}\frac{[Ca^{2+}]^3}{[Al^{3+}]^2}, \quad \frac{f_{Ca}}{f_{Mg}} = K_{Ca-Mg}\frac{[Ca^{2+}]}{[Mg^{2+}]}, \quad \frac{f_{Ca}}{f_K^2} = K_{Ca-K}\frac{[Ca^{2+}]}{[K^+]^2}, \tag{A5}$$

where the exchange equations for Ca-Na and Ca-H are equivalent to Ca-K. The soil-dependent cation exchange constants can be evaluated with coupled measurements of adsorbed and dissolved species or can be evaluated after the extensive dataset of Vries and Posch (2003). The sum of all exchangeable fractions (f) is equal to unity, namely

$$f_{Ca} + f_{Al} + f_{Mg} + f_{Na} + f_K + f_H = 1. \tag{A6}$$

Air-Water Carbonate System. In the soil solutions, and more generally in natural waters, the alkalinity charge difference expressed in (A4) is balanced by the aqueous carbonate system

$$[Alk] = [HCO_3^-] + 2[CO_3^{2-}] + [OH^-] - [H^+], \tag{A7}$$

$$[DIC] = [CO_2]_w + [HCO_3^-] + [CO_3^{2-}] \tag{A8}$$

$$[HCO_3^-] = K_1[CO_2]_w/[H^+], \qquad [CO_3^{2-}] = K_1 K_2[CO_2]_w/[H^+]^2, \tag{A9}$$

$$[CO_2]_a = K_H[CO_2]_w, \qquad [OH^-] = [H^+]/K_w, \tag{A10}$$

where K_1 and K_2 are the first and second carbonic acid dissociation constants. K_w is the water dissociation constant. K_H is Henry's constant for CO_2 solubility. All these constants and their temperature dependence are evaluated after (Stumm & Morgan, 1996). The combination of Eqs. (A4) and (A7) summarize EW goal of increasing alkalinity by mineral dissolution to promote aqueous carbonate formation. The efficiency of this process varies as a function of the water chemistry (Bertagni & Porporato, 2022). Formal
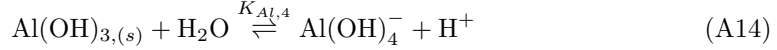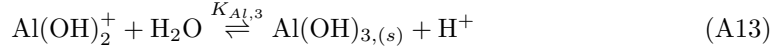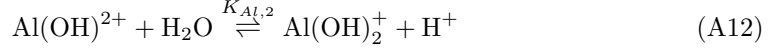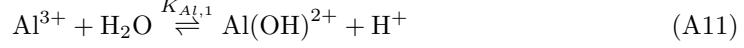
extension to the alkalinity definition (A7) could include aluminum, which plays a buffer role in acidic conditions, and organic alkalinity. Other weak acids and bases have been shown to play a negligible role in the soil solution (Bertagni & Porporato, 2022).

Aluminum Speciation. Aluminum chemistry is complex and strongly influenced by water pH (Weil & Brady, 2016; Nordstrom & May, 2020). Aluminum in aqueous systems speciates into five main monomeric species, following the reactions

$$Al^{3+} + H_2O \overset{K_{Al,1}}{\rightleftharpoons} Al(OH)^{2+} + H^+ \tag{A11}$$

$$Al(OH)^{2+} + H_2O \overset{K_{Al,2}}{\rightleftharpoons} Al(OH)_2^+ + H^+ \tag{A12}$$

$$Al(OH)_2^+ + H_2O \overset{K_{Al,3}}{\rightleftharpoons} Al(OH)_{3,(s)} + H^+ \tag{A13}$$

$$Al(OH)_{3,(s)} + H_2O \overset{K_{Al,4}}{\rightleftharpoons} Al(OH)_4^- + H^+ \tag{A14}$$

where the constants K_{Al} are evaluated after Weil and Brady (2016). In highly acidic (pH< 4.5) and highly alkaline (pH> 7) conditions, aluminum solubility is enhanced, and the dominant species are dissolved Al^{3+} and $Al(OH)_4^-$, respectively. By contrast, at intermediate pH values (5 <pH< 7), Al is present in less mobile forms, such as the hydroxy aluminum ions $Al(OH)^{2+}$ and $Al(OH)_2^+$, which typically form complexes with organic matter and other soil elements, as well as the solid mineral gibbsite $Al(OH)_3$. We hence discriminate into mobile ($[Al]_{mob}$) and immobile (Al_{imm}) aluminum pools following

$$[Al]_{mob} = [Al^{3+}] + [Al(OH)_4^-], \tag{A15}$$

$$Al_{imm} = ([Al(OH)^{2+}] + [Al(OH)_2^+] + [Al(OH)_3])nZ_r s. \tag{A16}$$

We then consider that only the mobile Al can be lost through leaching events; see eq. (8).

Appendix B Plants dynamics and their role in EW

Plants influence enhanced weathering dynamics by impacting soil hydrological and biogeochemical balances. Plant roots transpire water, actively and passively uptake nutrients, and release inorganic carbon (autotrophic respiration). In the model, growing vegetation (V) can be dynamically modeled through a classical logistic equation

$$\frac{dV}{dt} = \alpha_V V(k_V - V), \tag{B1}$$

where k_V is the carrying capacity per unit area, dependent on plant and ecosystem types, and α_V is the plant growth rate. The growth rate can be estimated based on the time (t_V) required for plants to progress from seedling to maturity through $\alpha_V \approx 6/t_V$. Simulated plant-mediated processes are then scaled with the normalized vegetation variable $\hat{V} = V/k_V$, defined between 0 and 1. These processes include: i) plant transpiration (T), modeled as a soil moisture function (Laio et al., 2001a); ii) plant passive uptake, assumed to be directly proportional to the transpiration rate (Cipolla et al., 2021a); iii) autotrophic respiration ($RESP_a$), estimated to be equivalent to heterotrophic respiration when plants are fully grown (Bond-Lamberty et al., 2004); iv) active uptake, which occurs during plant growth when passive uptake alone cannot meet the nutrient demands for growth (see below). Noteworthy, both plant-mediated nutrient uptake and inorganic carbon release processes contribute to soil acidification.

In addition to the nutrient uptake through the transpiration stream (passive uptake), plants can also rely on more complex and energetically expensive physiological processes (active uptake) when the passive uptake is insufficient to meet the nutrient demand (DEM). The active uptake then counts on a diffusion flux from the bulk of the solution to the plant roots (Porporato, D'Odorico, et al., 2003; Porporato & Yin, 2022).

Here we propose a new modeling framework for the plant active uptake wherein the diffusive flux is quantified by the root surface area (i.e., the root area index, RAI), the element diffusivity in water (D_{w}), and the concentration gradient between the root surface and the solution bulk. Assuming a null element concentration on the root surface and taking calcium (Ca) as an example, the concentration gradient is $[\mathrm{Ca}]/\ell$, where ℓ is the typical distance traveled from bulk to root. The latter can be quantified as $\ell = \sqrt{\mathrm{r}_d Z/(\hat{V} \cdot \mathrm{RAI})}$, assuming parallel cylindrical roots of average diameter d_r uniformly distributed over the depth Z (Manzoni et al., 2013) and considering that the root surface area scales with the vegetation stage. Active uptake for Ca can then be expressed as

$$\mathrm{UP}_{\mathrm{Ca}} = \begin{cases} 0 & \text{if } [\mathrm{Ca}]T \geq \mathrm{DEM}_{\mathrm{Ca}} \\ \min\left(\hat{V} \cdot \mathrm{RAI} \cdot D_{\mathrm{w}} \frac{[\mathrm{Ca}]}{\ell}, \mathrm{DEM}_{\mathrm{Ca}} - T[\mathrm{Ca}]\right) & \text{if } [\mathrm{Ca}]T < \mathrm{DEM}_{\mathrm{Ca}} \end{cases} \tag{B2}$$

$\mathrm{DEM}_{\mathrm{Ca}}$ defines the calcium required for the plant's new biomass development ($\mathrm{DEM}_{\mathrm{Ca}} = \xi_{\mathrm{Ca}} dV/dt$), with ξ_{Ca} being a plant-dependent coefficient specifying moles of Ca per biomass unit. Similar equations apply to other essential plant nutrients, including Mg, K, and Si.

Acknowledgments

References

Allen, R. G., Pereira, L. S., Raes, D., & Smith, M. (Eds.). (1998). *Crop evapotranspiration: guidelines for computing crop water requirements* (No. 56). Rome: Food and Agriculture Organization of the United Nations.

Amann, T., & Hartmann, J. (2022). Carbon Accounting for Enhanced Weathering. *Frontiers in Climate*, *4*. Retrieved 2022-05-10, from `https://www.frontiersin.org/article/10.3389/fclim.2022.849948`

Amann, T., Hartmann, J., Struyf, E., de Oliveira Garcia, W., Fischer, E. K., Janssens, I., ... Schoelynck, J. (2020, January). Enhanced Weathering and related element fluxes – a cropland mesocosm approach. *Biogeosciences*, *17*(1), 103–119. Retrieved 2021-06-22, from `https://bg.copernicus.org/articles/17/103/2020/` doi: 10.5194/bg-17-103-2020

Baek, S. H., Kanzaki, Y., Lora, J. M., Planavsky, N., Reinhard, C. T., & Zhang, S. (2023). Impact of Climate on the Global Capacity for Enhanced Rock Weathering on Croplands. *Earth's Future*, *11*(8), e2023EF003698. Retrieved 2023-11-21, from `https://onlinelibrary.wiley.com/doi/abs/10.1029/2023EF003698` (_eprint: https://onlinelibrary.wiley.com/doi/pdf/10.1029/2023EF003698) doi: 10.1029/2023EF003698

Beerling, D. J., Kantzas, E. P., Lomas, M. R., Wade, P., Eufrasio, R. M., Renforth, P., ... Banwart, S. A. (2020, July). Potential for large-scale CO2 removal via enhanced rock weathering with croplands. *Nature*, *583*(7815), 242–248. Retrieved 2021-06-22, from `http://www.nature.com/articles/s41586-020-2448-9` doi: 10.1038/s41586-020-2448-9

Berge, H. F. M. t., Meer, H. G. v. d., Steenhuizen, J. W., Goedhart, P. W., Knops, P., & Verhagen, J. (2012, August). Olivine Weathering in Soil, and Its Effects on Growth and Nutrient Uptake in Ryegrass (Lolium perenne L.): A Pot Experiment. *PLOS ONE*, *7*(8), e42098. Retrieved 2022-03-30, from `https://journals.plos.org/plosone/article?id=10.1371/journal.pone.0042098` (Publisher: Public Library of Science) doi: 10.1371/journal.pone.0042098

Bertagni, M. B., & Porporato, A. (2022, September). The Carbon-Capture Efficiency of Natural Water Alkalinization: Implications For Enhanced weathering. *Science of The Total Environment*, *838*, 156524. Retrieved 2022-06-15, from `https://www.sciencedirect.com/science/article/pii/S004896972203621X` doi: 10.1016/j.scitotenv.2022.156524

Blanc-Betes, E., Kantola, I. B., Gomez-Casanovas, N., Hartman, M. D., Parton, W. J., Lewis, A. L., . . . DeLucia, E. H. (2021). In silico assessment of the potential of basalt amendments to reduce N2O emissions from bioenergy crops. *GCB Bioenergy*, *13*(1), 224–241. Retrieved 2022-05-03, from `https://onlinelibrary.wiley.com/doi/abs/10.1111/gcbb.12757` (_eprint: https://onlinelibrary.wiley.com/doi/pdf/10.1111/gcbb.12757) doi: 10.1111/gcbb.12757

Bleam, W. F. (2017). *Soil and environmental chemistry* (Second edition ed.). Amsterdam ; Boston: Elsevier/AP, Academic Press is an imprint of Elsevier.

Bond-Lamberty, B., Wang, C., & Gower, S. T. (2004). A global relationship between the heterotrophic and autotrophic components of soil respiration? *Global Change Biology*, *10*(10), 1756–1766. Retrieved 2023-10-24, from `https://onlinelibrary.wiley.com/doi/abs/10.1111/j.1365-2486.2004.00816.x` (_eprint: https://onlinelibrary.wiley.com/doi/pdf/10.1111/j.1365-2486.2004.00816.x) doi: 10.1111/j.1365-2486.2004.00816.x

Buckingham, F. L., Henderson, G. M., Holdship, P., & Renforth, P. (2022, December). Soil core study indicates limited CO2 removal by enhanced weathering in dry croplands in the UK. *Applied Geochemistry*, *147*, 105482. Retrieved 2023-10-04, from `https://www.sciencedirect.com/science/article/pii/S0883292722002864` doi: 10.1016/j.apgeochem.2022.105482

Calabrese, S., & Porporato, A. (2020, September). Wetness controls on global chemical weathering. *Environmental Research Communications*, *2*(8), 085005. Retrieved 2021-06-22, from `https://iopscience.iop.org/article/10.1088/2515-7620/abad7b` doi: 10.1088/2515-7620/abad7b

Calabrese, S., Wild, B., Bertagni, M. B., Bourg, I. C., White, C., Aburto, F., . . . Porporato, A. (2022, October). Nano- to Global-Scale Uncertainties in Terrestrial Enhanced Weathering. *Environmental Science & Technology*. Retrieved 2022-10-24, from `https://doi.org/10.1021/acs.est.2c03163` (Publisher: American Chemical Society) doi: 10.1021/acs.est.2c03163

Calvin, K., Dasgupta, D., Krinner, G., Mukherji, A., Thorne, P. W., Trisos, C., . . . Péan, C. (2023, July). *IPCC, 2023: Climate Change 2023: Synthesis Report. Contribution of Working Groups I, II and III to the Sixth Assessment Report of the Intergovernmental Panel on Climate Change [Core Writing Team, H. Lee and J. Romero (eds.)]. IPCC, Geneva, Switzerland.* (Tech. Rep.). Intergovernmental Panel on Climate Change (IPCC). Retrieved 2023-11-22, from `https://www.ipcc.ch/report/ar6/syr/` (Edition: First) doi: 10.59327/IPCC/AR6-9789291691647

Cipolla, G., Calabrese, S., Noto, L. V., & Porporato, A. (2021a, August). The role of hydrology on enhanced weathering for carbon sequestration II. From hydroclimatic scenarios to carbon-sequestration efficiencies. *Advances in Water Resources*, *154*, 103949. Retrieved 2021-06-22, from `https://linkinghub.elsevier.com/retrieve/pii/S0309170821001044` doi: 10.1016/j.advwatres.2021.103949

Cipolla, G., Calabrese, S., Noto, L. V., & Porporato, A. (2021b, May). The role

of hydrology on enhanced weathering for carbon sequestration I. Modeling rock-dissolution reactions coupled to plant, soil moisture, and carbon dynamics. *Advances in Water Resources*, 103934. Retrieved 2021-06-22, from `https://linkinghub.elsevier.com/retrieve/pii/S0309170821000890` doi: 10.1016/j.advwatres.2021.103934

Clarkson, M. O., Larkin, C., Swoboda, P., Reershemius, T., Suhrhoff, J. T., Maesano, C. N., & Campbell, J. (2023, November). A Review of Measurement for Quantification of Carbon Dioxide Removal by Enhanced Weathering in Soil. Retrieved 2023-12-01, from `https://eartharxiv.org/repository/view/6317/` (Publisher: EarthArXiv)

Deng, K., Yang, S., & Guo, Y. (2022, April). A global temperature control of silicate weathering intensity. *Nature Communications*, *13*(1), 1781. Retrieved 2023-10-23, from `https://www.nature.com/articles/s41467-022-29415-0` (Number: 1 Publisher: Nature Publishing Group) doi: 10.1038/s41467-022-29415-0

Dietzen, C., Harrison, R., & Michelsen-Correa, S. (2018, July). Effectiveness of enhanced mineral weathering as a carbon sequestration tool and alternative to agricultural lime: An incubation experiment. *International Journal of Greenhouse Gas Control*, *74*, 251–258. Retrieved 2022-03-28, from `https://www.sciencedirect.com/science/article/pii/S1750583618300057` doi: 10.1016/j.ijggc.2018.05.007

Dietzen, C., & Rosing, M. T. (2023, May). Quantification of CO2 uptake by enhanced weathering of silicate minerals applied to acidic soils. *International Journal of Greenhouse Gas Control*, *125*, 103872. Retrieved 2023-11-20, from `https://www.sciencedirect.com/science/article/pii/S1750583623000427` doi: 10.1016/j.ijggc.2023.103872

Dong, X., Richter, D. D., Thompson, A., & Wang, J. (2023, December). The primacy of temporal dynamics in driving spatial self-organization of soil iron redox patterns. *Proceedings of the National Academy of Sciences*, *120*(51), e2313487120. Retrieved 2023-12-22, from `https://www.pnas.org/doi/abs/10.1073/pnas.2313487120` (Publisher: Proceedings of the National Academy of Sciences) doi: 10.1073/pnas.2313487120

Dupla, X., Möller, B., Baveye, P. C., & Grand, S. (2023). Potential accumulation of toxic trace elements in soils during enhanced rock weathering. *European Journal of Soil Science*, *74*(1), e13343. Retrieved 2023-11-10, from `https://onlinelibrary.wiley.com/doi/abs/10.1111/ejss.13343` (_eprint: https://onlinelibrary.wiley.com/doi/pdf/10.1111/ejss.13343) doi: 10.1111/ejss.13343

Fauteux, F., Rémus-Borel, W., Menzies, J. G., & Bélanger, R. R. (2005, August). Silicon and plant disease resistance against pathogenic fungi. *FEMS Microbiology Letters*, *249*(1), 1–6. Retrieved 2023-12-20, from `https://doi.org/10.1016/j.femsle.2005.06.034` doi: 10.1016/j.femsle.2005.06.034

Hamilton, S. K., Kurzman, A. L., Arango, C., Jin, L., & Robertson, G. P. (2007, June). Evidence for carbon sequestration by agricultural liming: FATE OF CARBON IN AGRICULTURAL LIME. *Global Biogeochemical Cycles*, *21*(2), n/a–n/a. Retrieved 2021-06-22, from `http://doi.wiley.com/10.1029/2006GB002738` doi: 10.1029/2006GB002738

Haque, F., Chiang, Y. W., & Santos, R. M. (2020, June). Risk assessment of Ni, Cr, and Si release from alkaline minerals during enhanced weathering. *Open Agriculture*, *5*(1), 166–175. Retrieved 2021-06-22, from `https://www.degruyter.com/document/doi/10.1515/opag-2020-0016/html` doi: 10.1515/opag-2020-0016

Hartmann, J., West, A. J., Renforth, P., Köhler, P., De La Rocha, C. L., Wolf-Gladrow, D. A., … Scheffran, J. (2013, April). Enhanced chemical weathering as a geoengineering strategy to reduce atmospheric carbon dioxide, supply nutrients, and mitigate ocean acidification: ENHANCED WEATH-

ERING. *Reviews of Geophysics*, *51*(2), 113–149. Retrieved 2021-06-22, from `http://doi.wiley.com/10.1002/rog.20004` doi: 10.1002/rog.20004

Jha, A., Bonetti, S., Smith, A. P., Souza, R., & Calabrese, S. (2023). Linking Soil Structure, Hydraulic Properties, and Organic Carbon Dynamics: A Holistic Framework to Study the Impact of Climate Change and Land Management. *Journal of Geophysical Research: Biogeosciences*, *128*(7), e2023JG007389. Retrieved 2023-12-23, from `https://onlinelibrary.wiley.com/doi/abs/10.1029/2023JG007389` (_eprint: https://onlinelibrary.wiley.com/doi/pdf/10.1029/2023JG007389) doi: 10.1029/2023JG007389

Jury, W. A., & Horton, R. (2004). *Soil Physics*. John Wiley & Sons. (Google-Books-ID: E5HZDwAAQBAJ)

Kantzas, E. P., Val Martin, M., Lomas, M. R., Eufrasio, R. M., Renforth, P., Lewis, A. L., ... Beerling, D. J. (2022, April). Substantial carbon drawdown potential from enhanced rock weathering in the United Kingdom. *Nature Geoscience*, 1–8. Retrieved 2022-05-03, from `https://www.nature.com/articles/s41561-022-00925-2` (Publisher: Nature Publishing Group) doi: 10.1038/s41561-022-00925-2

Kelland, M. E., Wade, P. W., Lewis, A. L., Taylor, L. L., Sarkar, B., Andrews, M. G., ... Beerling, D. J. (2020, June). Increased yield and CO2 sequestration potential with the C4cereal-Sorghum bicolor-cultivated in basaltic rock dust-amended agricultural soil. *Global Change Biology*, *26*(6), 3658–3676. Retrieved 2021-06-22, from `https://onlinelibrary.wiley.com/doi/10.1111/gcb.15089` doi: 10.1111/gcb.15089

Kim, Y.-H., Khan, A. L., Kim, D.-H., Lee, S.-Y., Kim, K.-M., Waqas, M., ... Lee, I.-J. (2014, January). Silicon mitigates heavy metal stress by regulating P-type heavy metal ATPases, Oryza sativalow silicon genes, and endogenous phytohormones. *BMC Plant Biology*, *14*(1), 13. Retrieved 2023-12-20, from `https://doi.org/10.1186/1471-2229-14-13` doi: 10.1186/1471-2229-14-13

Kirk, G. J. D., Versteegen, A., Ritz, K., & Milodowski, A. E. (2015, September). A simple reactive-transport model of calcite precipitation in soils and other porous media. *Geochimica et Cosmochimica Acta*, *165*, 108–122. Retrieved 2023-10-24, from `https://www.sciencedirect.com/science/article/pii/S0016703715003075` doi: 10.1016/j.gca.2015.05.017

Klemme, A., Rixen, T., Müller, M., Notholt, J., & Warneke, T. (2022, September). Destabilization of carbon in tropical peatlands by enhanced weathering. *Communications Earth & Environment*, *3*(1), 1–9. Retrieved 2023-02-03, from `https://www.nature.com/articles/s43247-022-00544-0` (Number: 1 Publisher: Nature Publishing Group) doi: 10.1038/s43247-022-00544-0

Knapp, W. J., Stevenson, E. I., Renforth, P., Ascough, P. L., Knight, A. C. G., Bridgestock, L., ... Tipper, E. T. (2023, July). Quantifying CO2 Removal at Enhanced Weathering Sites: a Multiproxy Approach. *Environmental Science & Technology*, *57*(26), 9854–9864. Retrieved 2023-11-03, from `https://doi.org/10.1021/acs.est.3c03757` (Publisher: American Chemical Society) doi: 10.1021/acs.est.3c03757

Kohler, P., Hartmann, J., & Wolf-Gladrow, D. A. (2010, November). Geoengineering potential of artificially enhanced silicate weathering of olivine. *Proceedings of the National Academy of Sciences*, *107*(47), 20228–20233. Retrieved 2021-06-22, from `http://www.pnas.org/cgi/doi/10.1073/pnas.1000545107` doi: 10.1073/pnas.1000545107

Laio, F., Porporato, A., Ridolfi, L., & Rodriguez-Iturbe, I. (2001a, February). Mean first passage times of processes driven by white shot noise. *Physical Review E*, *63*(3), 036105. Retrieved 2021-06-24, from `https://link.aps.org/doi/10.1103/PhysRevE.63.036105` doi: 10.1103/PhysRevE.63.036105

Laio, F., Porporato, A., Ridolfi, L., & Rodriguez-Iturbe, I. (2001b). Plants in

water-controlled ecosystems: active role in hydrologic processes and response to water stress II. Probabilistic soil moisture dynamics. *Advances in Water Resources*, 17.

Larkin, C. S., Andrews, M. G., Pearce, C. R., Yeong, K. L., Beerling, D. J., Bellamy, J., ... James, R. H. (2022). Quantification of CO2 removal in a large-scale enhanced weathering field trial on an oil palm plantation in Sabah, Malaysia. *Frontiers in Climate*, *4*. Retrieved 2023-03-10, from `https://www.frontiersin.org/articles/10.3389/fclim.2022.959229`

Lasaga, A. C. (1984, June). Chemical kinetics of water-rock interactions. *Journal of Geophysical Research: Solid Earth*, *89*(B6), 4009–4025. Retrieved 2021-06-22, from `http://doi.wiley.com/10.1029/JB089iB06p04009` doi: 10.1029/ JB089iB06p04009

Manzoni, S., Schimel, J. P., & Porporato, A. (2012, April). Responses of soil microbial communities to water stress: results from a meta-analysis. *Ecology*, *93*(4), 930–938. Retrieved 2021-06-22, from `https://onlinelibrary.wiley.com/ doi/10.1890/11-0026.1` doi: 10.1890/11-0026.1

Manzoni, S., Vico, G., Porporato, A., & Katul, G. (2013, January). Biological constraints on water transport in the soil–plant–atmosphere system. *Advances in Water Resources*, *51*, 292–304. Retrieved 2023-11-17, from `https:// www.sciencedirect.com/science/article/pii/S0309170812000711` doi: 10.1016/j.advwatres.2012.03.016

Miele, F., Benettin, P., Wang, S., Retti, I., Asadollahi, M., Frutschi, M., ... Rinaldo, A. (2023). Spatially Explicit Linkages Between Redox Potential Cycles and Soil Moisture Fluctuations. *Water Resources Research*, *59*(3), e2022WR032328. Retrieved 2023-11-28, from `https:// onlinelibrary.wiley.com/doi/abs/10.1029/2022WR032328` (_eprint: https://onlinelibrary.wiley.com/doi/pdf/10.1029/2022WR032328) doi: 10.1029/2022WR032328

Morel, F., Hering, J. G., & Morel, F. (1993). *Principles and applications of aquatic chemistry.* New York: Wiley.

Nordstrom, D. K., & May, H. M. (2020, April). Aqueous Equilibrium Data for Mononuclear Aluminum Species. In G. Sposito (Ed.), *The Environmental Chemistry of Aluminum* (2nd ed., pp. 39–80). CRC Press. Retrieved 2021-06-22, from `https://www.taylorfrancis.com/books/9780429612480/ chapters/10.1201/9780138736781-2` doi: 10.1201/9780138736781-2

Palandri, K. (2004). *Rate parameters of water-mineral interaction kinetics for application to geochemical modeling* (Open-File Report). USGS. (Series: Open-File Report)

Porporato, A., D'Odorico, P., Laio, F., & Rodriguez-Iturbe, I. (2003, January). Hydrologic controls on soil carbon and nitrogen cycles. I. Modeling scheme. *Advances in Water Resources*, *26*(1), 45–58. Retrieved 2021-06-22, from `https://linkinghub.elsevier.com/retrieve/pii/S0309170802000945` doi: 10.1016/S0309-1708(02)00094-5

Porporato, A., Laio, F., Ridolfi, L., Caylor, K. K., & Rodriguez-Iturbe, I. (2003, February). Soil moisture and plant stress dynamics along the kalahari precipitation gradient: KALAHARI SOIL MOISTURE AND DYNAMICAL PLANT STRESS. *Journal of Geophysical Research: Atmospheres*, *108*(D3), n/a–n/a. Retrieved 2021-06-22, from `http://doi.wiley.com/10.1029/2002JD002448` doi: 10.1029/2002JD002448

Porporato, A., & Yin, J. (2022). *Ecohydrology: dynamics of life and water in the critical zone.* Cambridge, United Kingdom: Cambridge university press.

Reershemius, T., Kelland, M. E., Jordan, J. S., Davis, I. R., D'Ascanio, R., Kalderon-Asael, B., ... Planavsky, N. J. (2023, November). Initial Validation of a Soil-Based Mass-Balance Approach for Empirical Monitoring of Enhanced Rock Weathering Rates. *Environmental Science & Technology*. Retrieved

2023-11-21, from `https://doi.org/10.1021/acs.est.3c03609` (Publisher: American Chemical Society) doi: 10.1021/acs.est.3c03609

Renforth, P. (2012, September). The potential of enhanced weathering in the UK. *International Journal of Greenhouse Gas Control*, *10*, 229–243. Retrieved 2021-06-22, from `https://linkinghub.elsevier.com/retrieve/pii/S1750583612001466` doi: 10.1016/j.ijggc.2012.06.011

Renforth, P., & Henderson, G. (2017, September). Assessing ocean alkalinity for carbon sequestration. *Reviews of Geophysics*, *55*(3), 636–674. Retrieved 2021-06-22, from `http://doi.wiley.com/10.1002/2016RG000533` doi: 10.1002/2016RG000533

Renforth, P., Pogge von Strandmann, P., & Henderson, G. (2015, October). The dissolution of olivine added to soil: Implications for enhanced weathering. *Applied Geochemistry*, *61*, 109–118. Retrieved 2021-09-22, from `https://linkinghub.elsevier.com/retrieve/pii/S0883292715001389` doi: 10.1016/j.apgeochem.2015.05.016

Rodríguez-Iturbe, I., D'Odorico, P., Porporato, A., & Ridolfi, L. (1999, January). Tree-grass coexistence in Savannas: The role of spatial dynamics and climate fluctuations. *Geophysical Research Letters*, *26*(2), 247–250. Retrieved 2021-06-22, from `http://doi.wiley.com/10.1029/1998GL900296` doi: 10.1029/1998GL900296

Schaller, J., Puppe, D., Kaczorek, D., Ellerbrock, R., & Sommer, M. (2021, February). Silicon Cycling in Soils Revisited. *Plants*, *10*(2), 295. Retrieved 2021-06-22, from `https://www.mdpi.com/2223-7747/10/2/295` doi: 10.3390/plants10020295

Strefler, J., Amann, T., Bauer, N., Kriegler, E., & Hartmann, J. (2018, March). Potential and costs of carbon dioxide removal by enhanced weathering of rocks. *Environmental Research Letters*, *13*(3), 034010. Retrieved 2021-06-22, from `https://iopscience.iop.org/article/10.1088/1748-9326/aaa9c4` doi: 10.1088/1748-9326/aaa9c4

Stumm, W., & Morgan, J. J. (1996). *Aquatic chemistry: chemical equilibria and rates in natural waters* (3rd ed ed.). New York: Wiley.

Taylor, L. L., Driscoll, C. T., Groffman, P. M., Rau, G. H., Blum, J. D., & Beerling, D. J. (2021, January). Increased carbon capture by a silicate-treated forested watershed affected by acid deposition. *Biogeosciences*, *18*(1), 169–188. Retrieved 2021-06-22, from `https://bg.copernicus.org/articles/18/169/2021/` doi: 10.5194/bg-18-169-2021

Taylor, L. L., Quirk, J., Thorley, R. M. S., Kharecha, P. A., Hansen, J., Ridgwell, A., . . . Beerling, D. J. (2016, April). Enhanced weathering strategies for stabilizing climate and averting ocean acidification. *Nature Climate Change*, *6*(4), 402–406. Retrieved 2021-06-22, from `http://www.nature.com/articles/nclimate2882` doi: 10.1038/nclimate2882

te Pas, E. E. E. M., Hagens, M., & Comans, R. N. J. (2023). Assessment of the enhanced weathering potential of different silicate minerals to improve soil quality and sequester CO2. *Frontiers in Climate*, *4*. Retrieved 2023-02-03, from `https://www.frontiersin.org/articles/10.3389/fclim.2022.954064`

Val Martin, M., Blanc-Betes, E., Fung, K. M., Kantzas, E. P., Kantola, I. B., Chiaravalloti, I., . . . Beerling, D. J. (2023, October). Improving nitrogen cycling in a land surface model (CLM5) to quantify soil N_2O, NO, and NH_3 emissions from enhanced rock weathering with croplands. *Geoscientific Model Development*, *16*(20), 5783–5801. Retrieved 2023-11-28, from `https://gmd.copernicus.org/articles/16/5783/2023/` (Publisher: Copernicus GmbH) doi: 10.5194/gmd-16-5783-2023

Vienne, A., Poblador, S., Portillo-Estrada, M., Hartmann, J., Ijiehon, S., Wade, P., & Vicca, S. (2022). Enhanced Weathering Using Basalt Rock Powder: Carbon Sequestration, Co-benefits and Risks in a Mesocosm Study With

Solanum tuberosum. *Frontiers in Climate*, *4*. Retrieved 2023-04-27, from `https://www.frontiersin.org/articles/10.3389/fclim.2022.869456`

Vries, W. d., & Posch, M. (2003). *Derivation of cation exchange constants for sand, loess, clay and peat soils on the basis of field measurements in the Netherlands* (Tech. Rep. No. 701). Wageningen: Alterra. Retrieved 2023-10-25, from `https://library.wur.nl/WebQuery/wurpubs/349403` (ISSN: 1566-7197)

Wang, J. J., Dodla, S. K., & Henderson, R. E. (2004, December). SOIL SILICON EXTRACTABILITY WITH SEVEN SELECTED EXTRACTANTS IN RELATION TO COLORIMETRIC AND ICP DETERMINATION. *Soil Science*, *169*(12), 861. Retrieved 2023-11-21, from `https://journals.lww.com/soilsci/Fulltext/2004/12000/Soil_Silicon_Extractability_With_Seven_Selected.5.aspx`

Weil, R. R., & Brady, N. (2016). *The nature and properties of soils* (Fifteenth edition ed.). Columbus: Pearson.

Wieder, W. R., Bonan, G. B., & Allison, S. D. (2013, October). Global soil carbon projections are improved by modelling microbial processes. *Nature Climate Change*, *3*(10), 909–912. Retrieved 2023-12-23, from `https://www.nature.com/articles/nclimate1951` (Number: 10 Publisher: Nature Publishing Group) doi: 10.1038/nclimate1951

Wolf-Gladrow, D. A., Zeebe, R. E., Klaas, C., Körtzinger, A., & Dickson, A. G. (2007). Total alkalinity: The explicit conservative expression and its application to biogeochemical processes. *Marine Chemistry*, 14.

Zhang, S., Planavsky, N. J., Katchinoff, J., Raymond, P. A., Kanzaki, Y., Reershemius, T., & Reinhard, C. T. (2022). River chemistry constraints on the carbon capture potential of surficial enhanced rock weathering. *Limnology and Oceanography*, *67*(S2), S148–S157. Retrieved 2023-01-31, from `https://onlinelibrary.wiley.com/doi/abs/10.1002/lno.12244` (_eprint: https://onlinelibrary.wiley.com/doi/pdf/10.1002/lno.12244) doi: 10.1002/lno.12244